Quantum nature of reactivity modification in vibrational polariton chemistry

Yaling Ke and Jeremy O. Richardson
Department of Chemistry and Applied Biosciences, ETH Zürich, 8093 Zürich, Switzerland

(*Electronic mail: yaling.ke@phys.chem.ethz.ch)

In this work, we present a mixed quantum–classical open quantum system dynamics method for studying rate modifications of ground-state chemical reactions in an optical cavity under vibrational strong coupling conditions. In this approach, the cavity radiation mode is treated classically with a mean-field nuclear force averaging over the remaining degrees of freedom, both within the system and the environment, which are handled quantum mechanically within the hierarchical equations of motion framework. Using this approach, we conduct a comparative analysis by juxtaposing the mixed quantum–classical results with fully quantum mechanical simulations. Through this comparison, we confirm the crucial role of the quantum nature of the cavity radiation mode in reproducing the resonant peak observed in the cavity frequency-dependent rate profile. In other words, it is crucial to explicitly consider the quantized photonic states in studying reactivity modification in vibrational polariton chemistry, as these phenomena stem from cavity-induced reaction pathways involving resonant energy exchanges between photons and molecular vibrational transitions.

I. INTRODUCTION

In the realm of vibrational strong coupling,[1–5] where the exchange of photons between molecular vibrations and cavity radiation modes outpaces any decay processes, recent experiments in Fabry–Pérot cavities have reported rate modifications in ground-state chemical reactions under resonant conditions.[6–19] These findings have catalyzed the emergence of a vibrant new field of research known as polariton chemistry, prompting further experimental inquiries into a broad spectrum of chemical reactions within microfluidic infrared optical cavities and spurring substantial theoretical investigations.[20–48] This burgeoning field not only provides a fresh new avenue for comprehending chemical reaction mechanisms at a fundamental level but also presents a novel technique for selectively steering chemical reactions in an inexpensive and non-intrusive manner. Such advancements hold the potential for profound impacts on both chemical and material science.

Thus far, studies employing classical rate theories or ring-polymer molecular dynamics simulations have struggled to accurately capture the shape resonance observed in the cavity frequency-dependent rate profile.[28–35] On the other hand, quantum dynamics simulations, performed in the single-molecule and few-molecule limit,[49–52] have demonstrated the ability to depict the correct resonance structure. Yet, the questions remain as to why classical approaches fall short, and to what extent quantum effects are involved in this resonant modification of the reaction rate inside the optical cavity.

In our recent quantum dynamical study of ground-state chemical reactions inside an infrared optical cavity,[51] we revealed that static quantum features such as zero-point energy and pure tunneling effects are not the major cause of the observed resonant rate peak. Moreover, we proposed a mechanistic insight into this resonant rate modification. Overall, the modification of chemical reactivity inside the cavity can be rationalized by the opening of cavity-induced intramolecular and intermolecular reaction pathways. A cavity-induced intramolecular reaction pathway involves two distinct energy exchange processes. Firstly, there are energy exchanges between molecular vibrations and the cavity radiation mode. This is the cause of the resonant condition, where the photon energy matches a dipole-allowed molecular vibrational transition. The second energy exchange occurs between the cavity radiation mode and its surrounding bath, facilitating the thermalization of the cavity mode and thus ensuring the sustainability of the former energy exchange process in the long run. Furthermore, the collective coupling of molecules to a resonant cavity mode can also initiate an intermolecular reaction pathway, which is a high-order effect with respect to the light–matter coupling strength. Thereby, vibrational heating in one molecule becomes linked to the vibrational cooling in another molecule, further contributing to the rate modification. These cavity-induced reaction pathways hinge on the quantized nature of both molecular vibrational states and cavity photonic states. Hence, it appears that a quantum-mechanical description of both cavity mode and molecular vibrations is imperative for accurately interpreting the resonant rate modification of chemical reactions inside an optical cavity.

To validate this hypothesis, we conduct a control study in this work. Specifically, we compare the results obtained from a mixed quantum–classical simulation with those from fully quantum-mechanical simulations. In the mixed quantum–classical approach, the cavity radiation mode is treated classically via mean-field forces, whereas all other degrees of freedom are treated quantum mechanically using the hierarchical equations of motion (HEOM) approach (see Ref. 53 and the literature therein). The mixed quantum–classical method does not recover the quantum–mechanical results, which thus confirms the critical role of the quantum nature of the cavity radiation field in the study of cavity-induced chemical reactions in the electronic ground state.

The remainder of this work is structured as follows: in Sec. II, we first present an open quantum system model for describing chemical reactions in an optical cavity, accounting for both solvent effects and cavity losses. Subsequently, we introduce the mixed quantum–classical approach, wherein molecular vibrational dynamics are treated quantum mechanically while cavity photonic dynamics are described classi-

https://doi.org/10.26434/chemrxiv-2024-nfmpk **ORCID:** https://orcid.org/0000-0001-6625-3981 Content not peer-reviewed by ChemRxiv. **License:** CC BY 4.0

cally. Moving on to Sec. III, we assess the significance of the quantum nature of the cavity radiation field in shaping the resonance peak structure observed in cavity-induced modifications of chemical reactivity. Lastly, in Sec. IV, we highlight the importance of our findings in advancing further theoretical exploration of polariton chemistry.

II. THEORY

A. Model

Chemical reactions occurring in a condensed phase inside an infrared optical cavity can be effectively described as an open quantum system model. In this model, the system of interest is coupled to multiple bosonic baths, with the overall Hamiltonian given by

$$H = H_{\mathrm{S}} + H_{\mathrm{E}}, \tag{1}$$

where H_{S} corresponds to the system and H_{E} to the environment.

We employ the Pauli–Fierz quantum electrodynamics Hamiltonian to characterize the cavity–molecule system, comprising a single reactive degree of freedom (DoF) of the molecule and an electromagnetic radiation mode confined within a Fabry–Pérot cavity. The system Hamiltonian, under the dipole gauge and the long-wavelength approximation (hereafter setting $\hbar = 1$), takes the form[46,49,54,55]

$$H_{\mathrm{S}} = \frac{p_{\mathrm{m}}^2}{2} + E_{\mathrm{b}}\left(\frac{x_{\mathrm{m}}^2}{a^2} - 1\right)^2 + \frac{p_{\mathrm{c}}^2}{2} + \frac{1}{2}\omega_{\mathrm{c}}^2\left(x_{\mathrm{c}} - \sqrt{\frac{2}{\omega_{\mathrm{c}}}}\eta_{\mathrm{c}}\vec{\mu}(x_{\mathrm{m}})\cdot\vec{e}\right)^2. \tag{2}$$

The first two terms and the last two terms are associated with the molecule (H_{m}) and the cavity radiation mode (H_{c}), respectively. The mass-weighted momentum and coordinate of the molecular mode are denoted by p_{m} and x_{m}. The molecule is characterized by a symmetric double-well model with two local minima at $x_{\mathrm{m}} = \pm a$ separated by a barrier height of E_b at the origin $x_{\mathrm{m}} = 0$. The cavity radiation mode is modeled as a harmonic oscillator with momentum p_{c}, coordinate q_{c}, and frequency ω_{c}. The light–matter coupling induces an equilibrium displacement in the cavity coordinate by $\sqrt{\frac{2}{\omega_{\mathrm{c}}}}\eta_{\mathrm{c}}\vec{\mu}(x_{\mathrm{m}})\cdot\vec{e}$. Here, $\vec{e}$ is a unit vector pointing in the direction of light polarization, $\vec{\mu}(x_{\mathrm{m}})$ is the molecular dipole moment operator projected onto the electronic ground state. The coupling strength is specified by the parameter $\eta_{\mathrm{c}} = \frac{1}{\omega_{\mathrm{c}}}\sqrt{\frac{\omega_{\mathrm{c}}}{2\varepsilon_0 V}}$, where ε_0 is the permittivity of the medium in the cavity, and V is the effective quantization volume of the electromagnetic mode.

To account for the influence of the solvent and the continuum of far-field electromagnetic modes outside the cavity, we consider an environment composed of two bosonic baths, $H_{\mathrm{E}} = H_{\mathrm{ph}} + H_{\mathrm{pt}}$, namely, a phonon bath for dissipative solvent DoFs and a photon bath for the cavity lossy environment. Each bath can be modeled as an ensemble of infinite harmonic oscillators,

$$H_\alpha = \sum_k \frac{P_{\alpha k}^2}{2} + \frac{1}{2}\omega_{\alpha k}^2\left(Q_{\alpha k} - \frac{c_{\alpha k}s_\alpha(x_{\mathrm{m}},x_{\mathrm{c}})}{\omega_{\alpha k}^2}\right)^2. \tag{3}$$

where $P_{\alpha k}$ and $Q_{\alpha k}$ represent the mass-weighted momentum and coordinate of the kth oscillator with the frequency $\omega_{\alpha k}$ in bath α ($\in \{\mathrm{ph},\mathrm{pt}\}$). Every oscillator in the bath is displaced by $c_{\alpha k}s_\alpha(x_{\mathrm{m}},x_{\mathrm{c}})/\omega_{\alpha k}^2$ due to its coupling to the system, where $c_{\alpha k}$ denotes the coupling strength and $s_\alpha(x_{\mathrm{m}},x_{\mathrm{c}})$ the coupling operator.

B. Quantum dynamics of molecular vibration and baths

To explore the validity of a classical treatment of the radiation field in cavity-induced chemical reactions, we introduce a mixed quantum–classical scheme, which is similar to the approach employed in Ref. 56 to study the bond rupture at the molecule–metal interface.

Within this framework, as depicted schematically in Fig. 1, the operators p_c and x_c in the Hamiltonian (see Sec. II A) for the cavity radiation mode are parameterized as the classical trajectories p_{c}^t and x_{c}^t, respectively. Meanwhile, all other DoFs remain in the quantum-mechanical domain, and the quantum dynamics are described by the density operator $\rho(p_{\mathrm{c}}^t,x_{\mathrm{c}}^t,t)$. We start with a factorized initial state between the molecular vibrational mode and the baths, $\rho(0) = \rho_{\mathrm{m}}(0)\otimes\prod_\alpha\rho_\alpha$, with each bath being in its thermal equilibrium at temperature T. To obtain the molecular reaction dynamics, we adopt the HEOM method. A key idea in the HEOM method involves the exponential expansion of the bath correlation function, defined as

$$C_\alpha(t) = \frac{1}{\pi}\int_{-\infty}^{\infty}\frac{e^{-i\omega t}}{1-e^{-\beta\omega}}J_\alpha(\omega)\mathrm{d}\omega = \Gamma_\alpha^2\sum_{p=0}\eta_{\alpha p}e^{-\gamma_{\alpha p}t}. \tag{4}$$

Here, $\beta = 1/k_{\mathrm{B}}T$ is the inverse temperature (k_{B} is the Boltzmann constant), and $J_\alpha(\omega)$ denotes the spectral density function

$$J_\alpha(\omega) = \frac{\pi}{2}\sum_k\frac{c_{\alpha k}^2}{\omega_{\alpha k}}\delta(\omega-\omega_{\alpha k}), \tag{5}$$

which encodes the statistical properties of bath α and its impact on the system dynamics. The strength of the system–bath coupling strength is quantified as $\Gamma_\alpha = \sqrt{\lambda_\alpha}$, where the reorganization energy λ_α is defined as

$$\lambda_\alpha = \sum_k\frac{c_{\alpha k}^2}{2\omega_{\alpha k}^2} = \frac{1}{\pi}\int_{-\infty}^{\infty}\frac{J(\omega)}{\omega}\mathrm{d}\omega. \tag{6}$$

To determine the expansion coefficients coefficients $\eta_{\alpha p}$ and exponents $\gamma_{\alpha p}$ in Eq. (4), various sum-over-pole schemes, as detailed in the literature, such as, Refs. 57 and 58, can be employed.

Following the decomposition of the correlation function in Eq. (4), one can introduce a series of auxiliary density operators (ADOs), denoted as $\rho^{\mathbf{n}}(p_{\mathrm{c}}^t,x_{\mathrm{c}}^t,t)$. Each ADO is specified

https://doi.org/10.26434/chemrxiv-2024-nfmpk **ORCID:** https://orcid.org/0000-0001-6625-3981 Content not peer-reviewed by ChemRxiv. **License:** CC BY 4.0

by a superindex $\mathbf{n} = (\cdots, n_{\alpha p}, \cdots)$, where $n_{\alpha p}$ is a non-negative integer and can be assigned as the occupation number of the pth effective dissipative boson in bath α. The equation of motion for the ADOs is given by

$$\begin{aligned}\frac{\partial \rho^{\mathbf{n}}(p_{\mathrm{c}}^t, x_{\mathrm{c}}^t, t)}{\partial t} =& -i\left[H_{\mathrm{S}}^{\mathrm{ren}}(p_{\mathrm{c}}^t, x_{\mathrm{c}}^t), \rho^{\mathbf{n}}(p_{\mathrm{c}}^t, x_{\mathrm{c}}^t, t)\right] + \sum_{\alpha p} n_{\alpha p}\gamma_{\alpha p}\rho^{\mathbf{n}}(p_{\mathrm{c}}^t, x_{\mathrm{c}}^t, t) + i\sum_{\alpha p}\sqrt{n_{\alpha p}+1}\Gamma_\alpha\left[s_\alpha(x_{\mathrm{m}}, x_{\mathrm{c}}^t), \rho^{\mathbf{n}^+_{\alpha p}}(p_{\mathrm{c}}^t, x_{\mathrm{c}}^t, t)\right] \\ &+ i\sum_{\alpha p}\sqrt{n_{\alpha p}}\Gamma_\alpha\left(\eta_{\alpha p} s_\alpha(x_{\mathrm{m}}, x_{\mathrm{c}}^t)\rho^{\mathbf{n}^-_{\alpha p}}(p_{\mathrm{c}}^t, x_{\mathrm{c}}^t, t) - \eta^*_{\alpha p}\rho^{\mathbf{n}^-_{\alpha p}}(p_{\mathrm{c}}^t, x_{\mathrm{c}}^t, t)s_\alpha(x_{\mathrm{m}}, x_{\mathrm{c}}^t)\right),\end{aligned} \tag{7}$$

where we have the normalized system Hamiltonian $H_{\mathrm{S}}^{\mathrm{ren}}(p_{\mathrm{c}}^t, x_{\mathrm{c}}^t) = H_{\mathrm{S}}(p_{\mathrm{c}}^t, x_{\mathrm{c}}^t) + \sum_\alpha \lambda_\alpha s_\alpha^2(x_{\mathrm{m}}, x_{\mathrm{c}}^t)$ and $\mathbf{n}^\pm_{\alpha p} = (\cdots, n_{\alpha p} \pm 1, \cdots)$.

By reformulating each ADO into a tensor in twin space and constructing an extended wavefunction encompassing all ADOs,[59–61]

$$\begin{aligned}|\Psi(p_{\mathrm{c}}^t, x_{\mathrm{c}}^t, t)\rangle =& \sum_{\mathbf{n}} |\rho^{\mathbf{n}}(p_{\mathrm{c}}^t, x_{\mathrm{c}}^t, t)\rangle\!\rangle \otimes |\mathbf{n}\rangle \\ =& \sum_{\mathbf{n}}\sum_{\nu_{\mathrm{m}}\nu'_{\mathrm{m}}} C^{\mathbf{n}}_{\nu_{\mathrm{m}}\nu'_{\mathrm{m}}}(p_{\mathrm{c}}^t, x_{\mathrm{c}}^t, t)|\nu_{\mathrm{m}}\nu'_{\mathrm{m}}\rangle \otimes |\mathbf{n}\rangle,\end{aligned} \tag{8}$$

we can recast Eq. (7) into a Schrödinger equation

$$i\frac{\mathrm{d}|\Psi(p_{\mathrm{c}}^t, x_{\mathrm{c}}^t, t)\rangle}{\mathrm{d}t} = \mathcal{H}(p_{\mathrm{c}}^t, x_{\mathrm{c}}^t)|\Psi(p_{\mathrm{c}}^t, x_{\mathrm{c}}^t, t)\rangle, \tag{9}$$

with a non-Hermitian super-Hamiltonian

$$\begin{aligned}\mathcal{H}(p_{\mathrm{c}}^t, x_{\mathrm{c}}^t) =& \hat{H}_{\mathrm{S}}^{\mathrm{ren}}(p_{\mathrm{c}}^t, x_{\mathrm{c}}^t) - \tilde{H}_{\mathrm{S}}^{\mathrm{ren}}(p_{\mathrm{c}}^t, x_{\mathrm{c}}^t) - i\sum_\alpha\sum_p \gamma_{\alpha p} b^+_{\alpha p} b_{\alpha p} \\ &+ \sum_\alpha\sum_p \Gamma_\alpha(s_\alpha(\hat{x}_{\mathrm{m}}, x_c^t) - s_\alpha(\tilde{x}_{\mathrm{m}}, x_{\mathrm{c}}^t))b_{\alpha p} \\ &+ \sum_\alpha\sum_p \Gamma_\alpha(\eta_{\alpha p} s_\alpha(\hat{x}_{\mathrm{m}}, x_{\mathrm{c}}^t) - \eta^*_{\alpha p} s_\alpha(\tilde{x}_{\mathrm{m}}, x_{\mathrm{c}}^t))b^+_{\alpha p}.\end{aligned} \tag{10}$$

Here, the molecular vibrational DoF is represented in twin space by two independent indices, ν_{m} and ν'_{m}. A pair of super-operators ($\hat{O}$ and $\tilde{O}$) are introduced, corresponding to an operator O in the molecular vibrational subspace. For instance, we have $\hat{x}_{\mathrm{m}} = x_{\mathrm{m}} \otimes I_{\mathrm{m}}$ and $\tilde{x}_{\mathrm{m}} = I_{\mathrm{m}} \otimes x_{\mathrm{m}}^\dagger$ for the coordinate operator x_{m}, where I_{m} is a unit operator in the molecular subspace. Further, we introduce a pair of creation and annihilation operators for effective dissipative bosons in bath, $b^+_{\alpha p}$ and $b_{\alpha p}$, which act on $|\mathbf{n}\rangle$ to yield $b^+_{\alpha p}|\mathbf{n}\rangle = \sqrt{n_{\alpha p}+1}|\mathbf{n}^+_{\alpha p}\rangle$ and $b_{\alpha p}|\mathbf{n}\rangle = \sqrt{n_{\alpha p}}|\mathbf{n}^-_{\alpha p}\rangle$.

To solve Eq. (9) efficiently, we utilize the matrix product state (MPS) decomposition[62,63] of the extended wavefunction $|\Psi(p_{\mathrm{c}}^t, x_{\mathrm{c}}^t, t)\rangle$, and the super-Hamiltonian $\mathcal{H}(p_{\mathrm{c}}^t, x_{\mathrm{c}}^t)$ is decomposed as the matrix product operator at each time point, along with a time-propagation scheme based on the time-dependent variational principle, as described in Refs. 64–66.

C. Classical dynamics of the cavity radiation mode

Instead of a quantum harmonic oscillator description, the cavity photonic mode is now characterized by the continuous phase-space variables p_{c}^t and x_{c}^t. Classical trajectories are generated based on Hamilton's equations of motion, as in the Ehrenfest method,[67,68] where the nuclear force is approximated under the mean-field assumption, obtained by tracing over the time-dependent density matrix $\rho(p_{\mathrm{c}}^t, x_{\mathrm{c}}^t, t)$. In this approach, the cavity photonic dynamics are governed by

$$\dot{x}_{\mathrm{c}}^t = p_{\mathrm{c}}^t; \tag{11a}$$

$$\begin{aligned}\dot{p}_{\mathrm{c}}^t =& -\mathrm{tr}\left\{\frac{\partial H(p_{\mathrm{c}}^t, x_{\mathrm{c}}^t)}{\partial x_{\mathrm{c}}^t}\rho(p_{\mathrm{c}}^t, x_{\mathrm{c}}^t, t)\right\} \\ =& -\mathrm{tr}_{\mathrm{m}}\left\{\frac{\partial H_{\mathrm{S}}^{\mathrm{ren}}(p_{\mathrm{c}}^t, x_{\mathrm{c}}^t)}{\partial x_{\mathrm{c}}^t}\rho^{\mathbf{0}}(p_{\mathrm{c}}^t, x_{\mathrm{c}}^t, t)\right\} \\ &- \sum_{\alpha p}\Gamma_\alpha \mathrm{tr}_{\mathrm{m}}\left\{\frac{\partial s_\alpha(x_{\mathrm{m}}, x_{\mathrm{c}}^t)}{\partial x_{\mathrm{c}}^t}\rho^{\mathbf{1}_{\alpha p}}(p_{\mathrm{c}}^t, x_{\mathrm{c}}^t, t)\right\} \\ =& -\langle\mathbb{I}_{\mathrm{m}}|\frac{\partial \hat{H}_{\mathrm{S}}^{\mathrm{ren}}(p_{\mathrm{c}}^t, x_{\mathrm{c}}^t)}{\partial x_{\mathrm{c}}^t}|\Psi^{\mathbf{n}=\mathbf{0}}(p_{\mathrm{c}}^t, x_{\mathrm{c}}^t, t)\rangle \\ &- \sum_{\alpha p}\Gamma_\alpha\langle\mathbb{I}_{\mathrm{m}}|\frac{\partial s_\alpha(\hat{x}_{\mathrm{m}}, x_{\mathrm{c}}^t)}{\partial x_{\mathrm{c}}^t}|\Psi^{\mathbf{n}=\mathbf{1}_{\alpha p}}(p_{\mathrm{c}}^t, x_{\mathrm{c}}^t, t)\rangle.\end{aligned} \tag{11b}$$

Here, $\mathrm{tr}\{\cdots\}$ denotes tracing over all quantum DoFs, including the molecular vibrational mode and all bosons in the baths, and the trace $\mathrm{tr}_{\mathrm{m}}\{\cdots\}$ is performed solely within the molecular vibrational subspace. The unit vector for the molecular vibrational mode in twin space is defined as $|\mathbb{I}_{\mathrm{m}}\rangle = \sum_{\nu_{\mathrm{m}}=\nu'_{\mathrm{m}}}|\nu_{\mathrm{m}}\nu'_{\mathrm{m}}\rangle$ and can be decomposed in the MPS format as the product of two rank-3 tensors

$$|\mathbb{I}_{\mathrm{m}}\rangle = I_{d_{\mathrm{m}}} I'_{d_{\mathrm{m}}}, \tag{12}$$

where $I_{d_{\mathrm{m}}}$ is a $1 \times d_{\mathrm{m}} \times d_{\mathrm{m}}$ tensor with elements $I_{d_{\mathrm{m}}}^{[1,k,l]} = \delta_{kl}$, and $I'_{d_{\mathrm{m}}}$ is a $d_{\mathrm{m}} \times 1 \times d_m$ tensor with elements $I'^{[k,1,l]}_{d_{\mathrm{m}}} = \delta_{kl}$. Here, d_{m} is the size of the molecular vibrational basis set. The zeroth-tier reduced wavefunction in the molecular subspace $|\Psi^{\mathbf{n}=\mathbf{0}}(p_{\mathrm{c}}^t, x_{\mathrm{c}}^t, t)\rangle = \langle\mathbf{n}=\mathbf{0}|\Psi(p_{\mathrm{c}}^t, x_{\mathrm{c}}^t, t)\rangle$ is obtained by projecting all effective dissipative bosons in the baths to the ground state, and the first-tier reduced wavefunction $|\Psi^{\mathbf{n}=\mathbf{1}_{\alpha p}}(p_{\mathrm{c}}^t, x_{\mathrm{c}}^t, t)\rangle = \langle\mathbf{n}=\mathbf{1}_{\alpha p}|\Psi(p_{\mathrm{c}}^t, x_{\mathrm{c}}^t, t)\rangle$ to the single excitation manifold with the excitation occurring at the pth effective mode in bath α. Further details regarding the derivation of Eq. (11) are provided in the supporting information (SI).

In this work, we integrate the equations of motion of the classical subsystem using the fourth-order Runge–Kutta

https://doi.org/10.26434/chemrxiv-2024-nfmpk **ORCID:** https://orcid.org/0000-0001-6625-3981 Content not peer-reviewed by ChemRxiv. **License:** CC BY 4.0

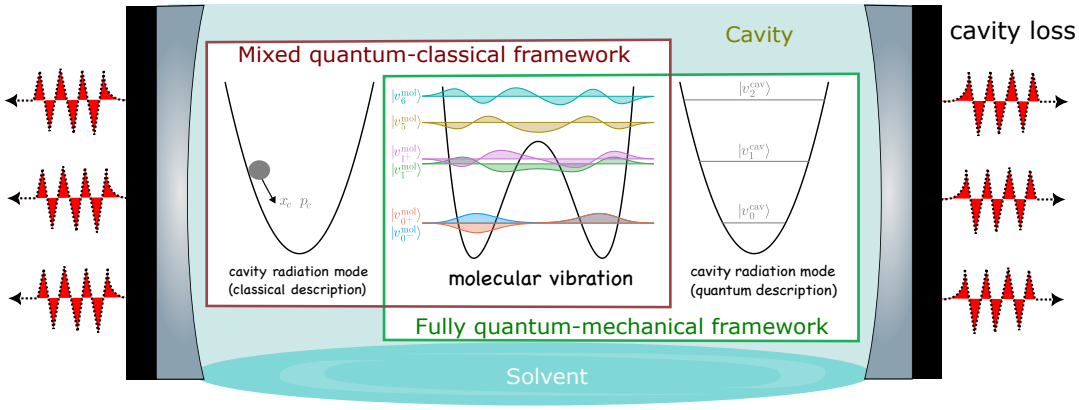

FIG. 1. Sketch of a chemical reaction occurring in a solvent within an optical cavity. The reactive mode is depicted by a double-well potential, and we show the lowest six eigenstates. Depending on whether we describe the cavity radiation mode classically using phase-space variables p_c and x_c, or quantum-mechanically using discrete states $|v_i^{\rm cav}\rangle$, we formulate either a mixed quantum–classical framework or fully quantum-mechanical framework.

method. The initial values for classical trajectories x_c^t and p_c^t are sampled from a Wigner distribution in the phase space,

$$W(p_c^0,x_c^0) = \frac{1}{2\pi\sigma_p\sigma_x}\exp-\frac{(p_c^0-\bar{p}_c)^2}{2\sigma_p^2}\exp-\frac{(x_c^0-\bar{x}_c)^2}{2\sigma_x^2}, \quad (13)$$

where $\bar{p}_c$ and $\bar{x}_c$ are the expectation values of the momentum and position, respectively, set to zero. The standard variances are given by

$$\sigma_x = \frac{1}{\sqrt{2\omega_c\tanh(\beta\omega_c/2)}}, \quad (14a)$$

$$\sigma_p = \sqrt{\frac{\omega_c}{2\tanh(\beta\omega_c/2)}}. \quad (14b)$$

It is worth noting that this mixed quantum–classical scheme can be easily generalized to an open quantum system, where a subset of vibrational DoFs are treated classically while the remaining DoFs are handled within the quantum-mechanical framework.

III. RESULTS

In all calculations presented below, we adopt E_b = 2250 cm^{-1}, a = 44.4 a.u., and the molecular dipole moment $u(x_m) = x_m$, oriented along the light polarization, consistent with previous studies.[34,43,49,50] The molecular vibration is described in the potential-optimized discrete variable representation,[69] and N_m = 12 lowest eigenstates are considered.

We assume a Lorentzian spectral density function for both the phonon and photon bath:

$$J_\alpha(\omega) = \frac{2\Gamma_\alpha^2\Omega_\alpha\omega}{\omega^2+\Omega_\alpha^2} \quad (15)$$

with the following parameters: Γ_{ph} = 100 cm^{-1}, Ω_{ph} = 200 cm^{-1}, Ω_{pt} = 1000 cm^{-1}, and a Γ_{pt} value yielding the cavity lifetime of $\tau_c = \frac{2J_{pt}(\omega_c)}{\omega_c(1-e^{-\beta\omega_c})}$ = 200 fs. The baths are maintained at room temperature T = 300 K, and each is simulated with four effective dissipative bosons per bath. The maximum occupation number $n_{\alpha p}$ per effective boson spans up to 10. For simplicity, we assume that the phonon bath exclusively interacts with the molecular vibration, characterized by $s_{ph}(x_m,x_c) = x_m$, while the photon bath couples solely to the cavity mode, represented by $s_{pt}(x_m,x_c) = x_c$. Additionally, we employ a maximal bond dimension D_{max} = 30 and a time step Δt = 0.5 fs.

The molecular vibrational and cavity photonic dynamics are obtained by solving the coupled equations of motion given by Eqs. (9) and (11). For each classical trajectory starting with p_c^0 and x_c^0, we initialize the molecular wavefunction with

$$|\Psi^{\mathbf{n}=\mathbf{0}}(p_c^0,x_c^0,0)\rangle = \frac{1}{Q}e^{-\beta H_m(p_c^0,x_c^0)/2}(1-h)e^{-\beta H_m(p_c^0,x_c^0)/2}, \quad (16)$$

where $Q = \mathrm{tr}_m\{e^{-\beta H_m(p_c^0,x_c^0)/2}(1-h)e^{-\beta H_m(p_c^0,x_c^0)/2}\}$, and

$$|\Psi^{\mathbf{n}\neq\mathbf{0}}(p_c^0,x_c^0,0)\rangle = 0. \quad (17)$$

Here, $h = \theta(x_m - x_m^\ddagger)$, defined as a Heaviside step function, is an operator projecting the wave packet onto the right side of a dividing surface $x_m^\ddagger$. For a single molecule with the symmetric double well potential as described in Sec. II A, we assume that the reactant and product region are separated by the dividing surface at $x_m^\ddagger = 0$. The reactant population in the left well region is thus computed as

$$\begin{aligned} P_r(t) &= \langle \mathrm{tr}\{(1-h)\rho(p_c^t,x_c^t,t)\}\rangle_{\rm traj} \\ &= 1 - \langle \mathrm{tr}_m\{h\rho^{\mathbf{0}}(p_c^t,x_c^t,t)\}\rangle_{\rm traj} \\ &= 1 - \langle \mathbb{I}_m|\hat{h}|\Psi^{\mathbf{n}=\mathbf{0}}(p_c^t,x_c^t,t)\rangle_{\rm traj}, \end{aligned} \quad (18)$$

https://doi.org/10.26434/chemrxiv-2024-nfmpk **ORCID:** https://orcid.org/0000-0001-6625-3981 Content not peer-reviewed by ChemRxiv. **License:** CC BY 4.0

where $\langle\cdots\rangle_{\text{traj}}$ denotes taking the average over classical trajectories. The time variation of the reactant population is related to the flux-side correlation function,

$$C^{\text{flux}}(t) = -\dot{P}_r(t) = \langle \text{tr}\{\rho(p_c^t, x_c^t, t)F\}\rangle_{\text{traj}} = \langle \mathbb{I}_m|\tilde{F}|\Psi^{\mathbf{n}=\mathbf{0}}(p_c^t, x_c^t, t)\rangle_{\text{traj}}, \tag{19}$$

where the flux operator is defined as $F = i[H, h]$.

In first-order reaction kinetics, the rigorous expression to calculate quantum rate constants in the flux correlation function formalism has been well established.[70–73] The forward reaction rate from the reactant region to the product region can be expressed as[71–73]

$$k = \lim_{t\to t_p} k(t) = \lim_{t\to t_p} \frac{C^{\text{flux}}(t)}{P_r(t) + (P_r(t) - 1)/K_{\text{eq}}}. \tag{20}$$

Here, assuming that the reaction exhibits rate-like behavior, there will be a plateau value of k, which is independent of the initial conditions. In Eq. (20), t_p is the time where $k(t)$ plateaus, and K_{eq} is the equilibrium constant, defined here as the ratio of the product and reactant population in the equilibrium state. For the symmetric model considered here, $K_{\text{eq}} = 1$.

It is important to note that we employ the full expression in Eq. (20) rather than the commonly used approximation $k \approx \lim_{t\to t_p} C^{\text{flux}}(t)$. The latter is equivalent to extracting the reaction rate from the slope of the time-dependent reactant population. However, this approximation only holds true for slow reactions when the molecule predominantly resides in the reactant regime at the time t_p where the transient oscillatory dynamics subside, i.e., $P_r(t_p) \approx 1$. As such, the denominator in Eq. (20) remains close to one and can be disregarded. This approximation does not hold for the model studied in the current and previous works.[34,43,49,50] This observation is true regardless of whether exact quantum-mechanical dynamics are used or the mixed quantum–classical approach. As an illustration, in Fig. 2(a), we compare the mixed quantum–classical $k(t)$ and flux-side correlation function $C^{\text{flux}}(t)$ for a reaction inside the cavity with the optical frequency $\omega_c = 1200\text{cm}^{-1}$. It is evident that after the short-time transient dynamics have decayed, $k(t)$ demonstrates a well-defined plateau, whereas $C^{\text{flux}}(t)$ does not.

Moreover, we compare the quantum–classical approximation to the reaction rate k and $C^{\text{flux}}(t)$ at $t = 10\,\text{ps}$ as a function of the cavity frequency in Fig. 2(b). We observe that while the former exhibits a monotonic increase with the optical frequency ω_c, the latter displays a dip centered at $\omega_c = 1185\,\text{cm}^{-1}$. This dip arises due to the lingering influence of the initial transient dynamics. To elaborate this, in Fig. 3(a), we illustrate the reactant dynamics for reactions outside and inside the cavity with three distinct optical frequencies. The solid lines correspond to the fully quantum-mechanical results, while the dotted lines represent the mixed quantum–classical results. Compared to the reaction outside the cavity, the reactant dynamics inside the cavity exhibit a more pronounced discontinuity in slopes around $t = 400\text{fs}$. Notably, the reactant population experiences the most significant short-time drop when on near resonance, i.e., the optical frequency

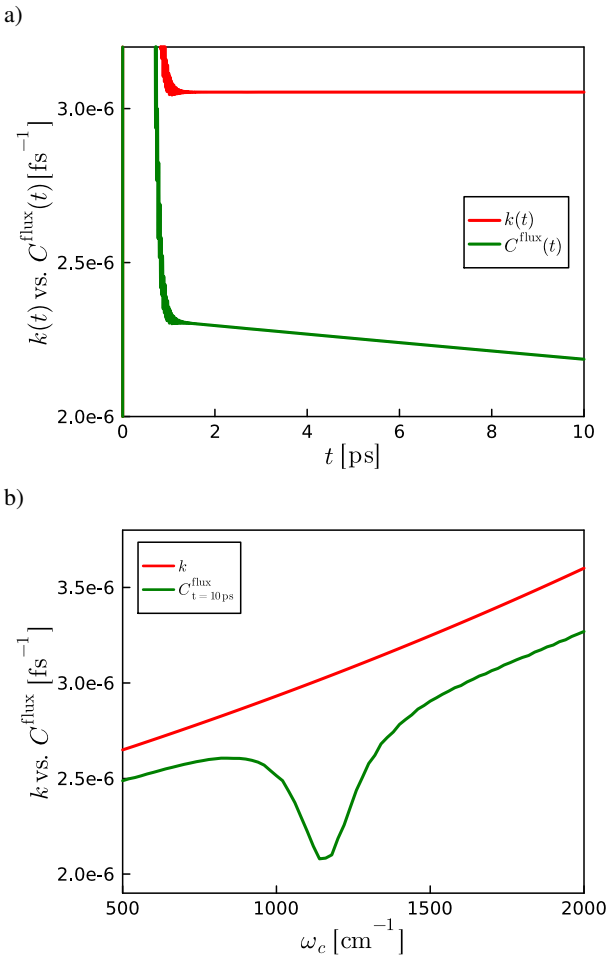

FIG. 2. a) Comparison of the mixed quantum–classical $k(t)$ and $C^{\text{flux}}(t)$ for a single molecule inside the cavity with the frequency $\omega_c = 1200\,\text{cm}^{-1}$. b) Reaction rates k and $C^{\text{flux}}(t = 10\,\text{ps})$ as a function of the cavity frequency. The light–matter coupling strength is set to $\eta_c = 0.005$ a.u. The results are obtained by averaging over 1000 classical trajectories.

is close to the transition energies $\Delta\varepsilon^{\text{mol}}_{0^+\leftrightarrow 1^-} = 1140\,\text{cm}^{-1}$ for the dipole-allowed molecular vibrational transition $|v^{\text{mol}}_{0^+}\rangle \to |v^{\text{mol}}_{1^-}\rangle$ and $\Delta\varepsilon^{\text{mol}}_{0^-\leftrightarrow 1^+} = 1238\,\text{cm}^{-1}$ for $|v^{\text{mol}}_{0^-}\rangle \to |v^{\text{mol}}_{1^+}\rangle$, and thus the photon energy can be absorbed. This short-time behavior may stem from the initial establishment of molecule–cavity correlation, which is factorized at $t = 0$. Further experiments, compatible with real-time spectroscopic monitoring,[74,75] may be able to directly track the polariton wavepacket on subpicosecond scales and probe the impact of the formation of this correlation. Moreover, the mixed quantum–classical treatment tends to overestimate this initial reactant reduction, as shown in Fig. 3(b), which compares the fully quantum-mechanical and mixed quantum–classical results for the short-time reactant population (at $t = 1\text{ps}$) as a function of ω_c.

Note that, a recent work employing various mixed quantum–classical methodologies,[43] where molecular vibrational mode is handled quantum mechanically while all other DoFs are treated classically, suggested that as long as discrete

https://doi.org/10.26434/chemrxiv-2024-nfmpk **ORCID:** https://orcid.org/0000-0001-6625-3981 Content not peer-reviewed by ChemRxiv. **License:** CC BY 4.0

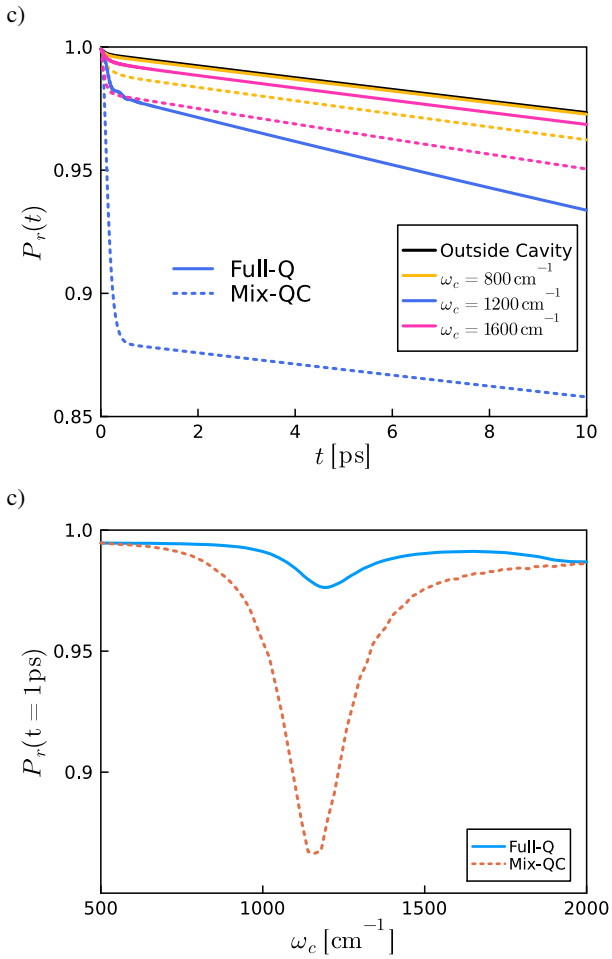

FIG. 3. a) Population dynamics of the reactant (in the left-well region) for a single molecule outside (black) and inside the cavity (colored) with three distinct cavity frequencies. b) Reactant population at time t = 1ps as a function of the optical frequency ω_c. The solid and dotted lines correspond to the mixed quantum–classical (Mix-QC) and fully quantum-mechanical (Full-Q) results, respectively. The light–matter coupling strength is set to η_c = 0.005 a.u. The mixed quantum–classical results are obtained by averaging over 1000 classical trajectories.

vibrational states are explicitly taken into account, a peak at the correct resonant photon frequency can be observed. However, the reaction rates obtained using these mixed quantum–classical approaches, both outside and inside the cavity, are orders of magnitude larger than the exact rates. Additionally, negative populations are occasionally observed. From the analysis provided earlier, these peaks might be spurious and originate from an inappropriate extraction of the reaction rate from the reactant dynamics.

In contrast to the short-time dynamics, the long-term rate k, as demonstrated in Fig. 2(b), exhibits a dependency on the cavity frequency but lacks a peak structure. This stands in stark contrast to the findings of the fully quantum-mechanical study.[49–51] To delve deeper into this disparity, we display in Fig. 4 the rate modification k/k_0 inside the cavity as a function of the cavity frequency for three different light–matter

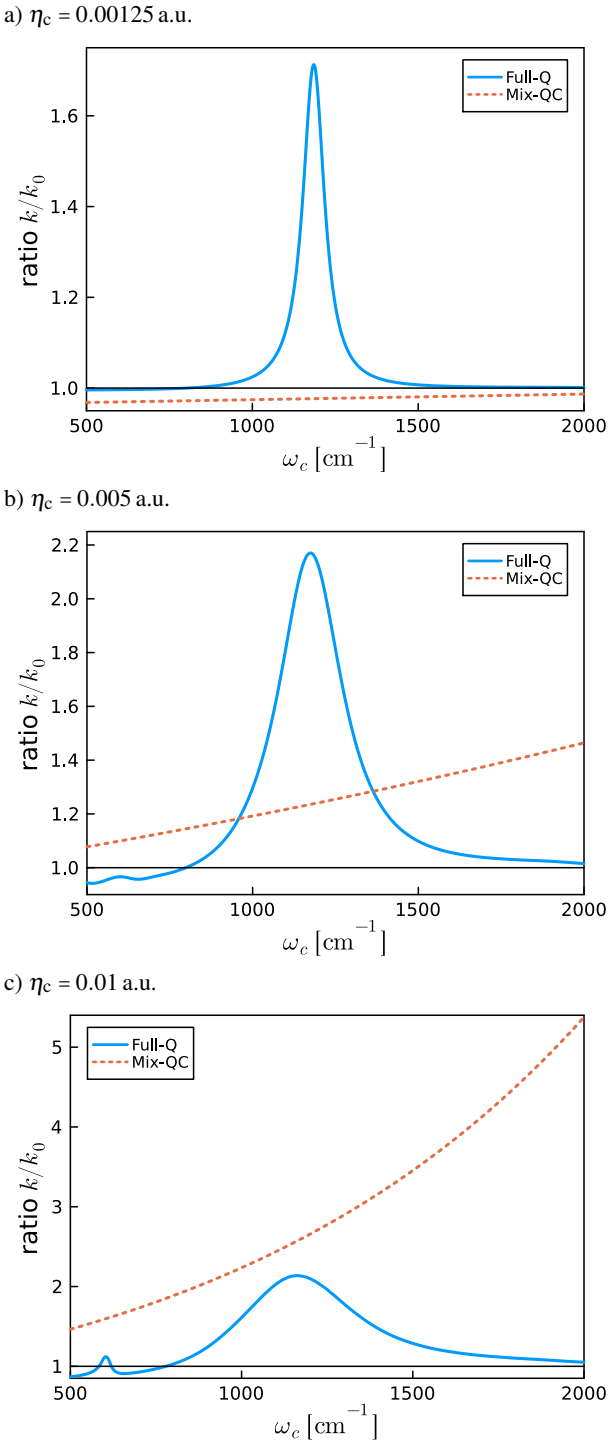

FIG. 4. Rate modification profile k/k_0 as a function of the cavity frequency ω_c for three different light-matter interaction strengths η_c. The blue solid lines represent the results obtained from the fully quantum-mechanical approach. The orange dotted lines correspond to the mixed quantum–classical treatment depicted in Sec. II, and the mixed quantum–classical results are obtained by averaging over 1000 classical optical trajectories.

https://doi.org/10.26434/chemrxiv-2024-nfmpk **ORCID:** https://orcid.org/0000-0001-6625-3981 Content not peer-reviewed by ChemRxiv. **License:** CC BY 4.0

coupling strengths η_c, directly comparing the results from both the fully quantum-mechanical method and the mixed quantum–classical approach. Here, k_0 is the reaction rate outside the cavity, which is by definition identical for both approaches.

For a light–matter coupling strength of $\eta_c = 0.00125\,\text{a.u.}$, corresponding to a Rabi splitting $\Omega_R \approx 30\,\text{cm}^{-1}$ for the vibrational transitions $|v_{0^\pm}^{\text{mol}}\rangle \to |v_{1^\mp}^{\text{mol}}\rangle$, the fully quantum-mechanical results display a sharp resonant peak centered at $\omega_c = 1185\text{cm}^{-1}$. As elucidated in Ref. 51, in the single-molecule limit, this resonant rate enhancement arises from the opening of an intramolecular reaction pathway, involving the molecular vibration, cavity mode, and its photon bath. The molecular vibrational transitions couple with the one-photon absorption/emission in the cavity mode, which is then quickly depleted/replenished by the photon bath to facilitate repeated occurrences of the former process. In comparison, the rates obtained with the mixed quantum–classical approach, where the cavity mode is treated classically, predict a slight reduction of the rates inside the cavity, devoid of any peak features.

In the regime of stronger light–matter coupling, the fully quantum-mechanical results exhibit a more intricate rate profile. For instance, the major resonant peak, in addition to its heightened intensity and further broadening, is flanked by a side peak in the low-frequency regime around $\omega_c = 600\,\text{cm}^{-1}$. This secondary peak corresponds to a multi-photon process where the emission/absorption of multiple photons in the cavity mode couples with the vibrational excitation/relaxation. The peak value varies, being higher or lower than one, depending on η_c. Conversely, the mixed quantum–classical results lack the peak features and instead predict rate enhancement inside the cavity across the whole frequency regime. Moreover, rates increase significantly in the high-frequency ω_c regime, possibly due to the larger dipole self-energy term $\omega_c \eta_c^2 x_m^2$.

Concluding from Fig. 4, we confirm our prediction that, it is crucial to employ a quantum description of the cavity radiation field for studying chemical reactivities under vibrational strong coupling conditions.

IV. CONCLUSION

In summary, we have introduced a mixed quantum–classical approach for modeling open bosonic systems. In this framework, a subset of vibrational modes can be treated classically, while the remaining DoFs, both within the system and its continuous baths, are handled quantum mechanically. This approach is instrumental for evaluating the dynamical quantum characteristics of specific vibrational modes.

In this work, our focus is on investigating the rate modification of ground-state chemical reactions inside an optical cavity. By exclusively treating the optical mode of the cavity classically, we have found that the resonant peak in the cavity frequency-dependent rate profile, observed in the fully quantum-mechanical simulations, is absent. This absence confirms our assumption that the resonant peak arises from a process involving the resonant energy exchange between the cavity mode and the molecular vibrations, which necessitates explicit consideration of both quantized cavity photonic states and discrete molecular vibrational states. Importantly, this finding strongly hints that the resonant rate alternation observed in vibrational strong coupling experiments inside optical cavities is essentially a macroscopic quantum phenomenon.

Nonetheless, this does not spell the end for mixed quantum–classical approaches. Although we will wish to treat the cavity mode quantum mechanically, there is probably no need to treat the entire system in this way. For instance, it is yet to be verified in future work whether the continuous dissipative bath modes can be treated classically. Finally, we must also consider the error inherent to the Ehrenfest mean-field approximation, which is well known to have a poor description of detailed balance.[76] In previous studies,[77,78] this approximation has been found to be significantly less accurate than alternative mixed quantum–classical methods such as spin mapping[79,80] and the mapping approach to surface hopping.[81] Therefore, in future work, we will investigate the possibility of combining HEOM with these more reliable approximations, which may overcome some of the errors observed with the Ehrenfest approximation in this work.

ACKNOWLEDGMENTS

The authors appreciate valuable discussions with Marit Fiechter.

SUPPLEMENTARY INFORMATION

See the supplementary material for the derivation details of Eq. (11).

DATA AVAILABILITY STATEMENT

The data that support the findings of this work are available from the corresponding author upon reasonable request.

CODE AVAILABILITY STATEMENT

The source code used in this study is available at https://github.com/yaling-ke/MixedQC_HEOMDynamics.jl

[1] T. W. Ebbesen, "Hybrid light–matter states in a molecular and material science perspective," Acc. Chem. Res. **49**, 2403–2412 (2016).
[2] K. Nagarajan, A. Thomas, and T. W. Ebbesen, "Chemistry under vibrational strong coupling," J. Am. Chem. Soc. **143**, 16877–16889 (2021).
[3] F. J. Garcia-Vidal, C. Ciuti, and T. W. Ebbesen, "Manipulating matter by strong coupling to vacuum fields," Science **373**, eabd0336 (2021).
[4] A. D. Dunkelberger, B. S. Simpkins, I. Vurgaftman, and J. C. Owrutsky, "Vibration-cavity polariton chemistry and dynamics," Annu. Rev. Phys. Chem. **73**, 429–451 (2022).
[5] A. Koner, M. Du, S. Pannir-Sivajothi, R. H. Goldsmith, and J. Yuen-Zhou, "A path towards single molecule vibrational strong coupling in a Fabry–Pérot microcavity," Chem. Sci. **14**, 7753–7761 (2023).

https://doi.org/10.26434/chemrxiv-2024-nfmpk **ORCID:** https://orcid.org/0000-0001-6625-3981 Content not peer-reviewed by ChemRxiv. **License:** CC BY 4.0

[6] A. Thomas, J. George, A. Shalabney, M. Dryzhakov, S. J. Varma, J. Moran, T. Chervy, X. Zhong, E. Devaux, C. Genet, et al., "Ground-state chemical reactivity under vibrational coupling to the vacuum electromagnetic field," Angew. Chem-ger. Edit. **128**, 11634–11638 (2016).

[7] R. M. Vergauwe, A. Thomas, K. Nagarajan, A. Shalabney, J. George, T. Chervy, M. Seidel, E. Devaux, V. Torbeev, and T. W. Ebbesen, "Modification of enzyme activity by vibrational strong coupling of water," Angew. Chem. - Int. Ed. **58**, 15324–15328 (2019).

[8] J. Lather, P. Bhatt, A. Thomas, T. W. Ebbesen, and J. George, "Cavity catalysis by cooperative vibrational strong coupling of reactant and solvent molecules," Angew. Chem. - Int. Ed. **58**, 10635–10638 (2019).

[9] A. Thomas, L. Lethuillier-Karl, K. Nagarajan, R. M. Vergauwe, J. George, T. Chervy, A. Shalabney, E. Devaux, C. Genet, J. Moran, et al., "Tilting a ground-state reactivity landscape by vibrational strong coupling," Science **363**, 615–619 (2019).

[10] H. Hiura, A. Shalabney, and J. George, "Vacuum-field catalysis: Accelerated reactions by vibrational ultra strong coupling," (2019).

[11] A. Thomas, A. Jayachandran, L. Lethuillier-Karl, R. M. Vergauwe, K. Nagarajan, E. Devaux, C. Genet, J. Moran, and T. W. Ebbesen, "Ground state chemistry under vibrational strong coupling: dependence of thermodynamic parameters on the rabi splitting energy," Proc. Spie. **9**, 249–255 (2020).

[12] K. Hirai, J. A. Hutchison, and H. Uji-i, "Recent progress in vibropolaritonic chemistry," ChemPlusChem **85**, 1981–1988 (2020).

[13] K. Hirai, R. Takeda, J. A. Hutchison, and H. Uji-i, "Modulation of prins cyclization by vibrational strong coupling," Angew. Chem-ger. Edit. **132**, 5370–5373 (2020).

[14] Y. Pang, A. Thomas, K. Nagarajan, R. M. Vergauwe, K. Joseph, B. Patrahau, K. Wang, C. Genet, and T. W. Ebbesen, "On the role of symmetry in vibrational strong coupling: the case of charge-transfer complexation," Angew. Chem. - Int. Ed. **59**, 10436–10440 (2020).

[15] A. Sau, K. Nagarajan, B. Patrahau, L. Lethuillier-Karl, R. M. Vergauwe, A. Thomas, J. Moran, C. Genet, and T. W. Ebbesen, "Modifying Woodward–Hoffmann stereoselectivity under vibrational strong coupling," Angew. Chem. - Int. Ed. **60**, 5712–5717 (2021).

[16] J. Lather, A. N. Thabassum, J. Singh, and J. George, "Cavity catalysis: modifying linear free-energy relationship under cooperative vibrational strong coupling," Chem. Sci. **13**, 195–202 (2022).

[17] W. Ahn, J. F. Triana, F. Recabal, F. Herrera, and B. S. Simpkins, "Modification of ground-state chemical reactivity via light–matter coherence in infrared cavities," Science **380**, 1165–1168 (2023).

[18] T. Ebbesen, B. Patrahau, M. Piejko, R. Mayer, C. Antheaume, T. Sangchai, G. Ragazzon, A. Jayachandran, E. Devaux, C. Genet, et al., "Direct observation of polaritonic chemistry by nuclear magnetic resonance spectroscopy," (2023).

[19] F. Gao, J. Guo, Q. Si, L. Wang, F. Zhang, and F. Yang, "Modification of atp hydrolysis by strong coupling with O-H stretching vibration," ChemPhotoChem **7**, e202200330 (2023).

[20] J. Galego, F. J. Garcia-Vidal, and J. Feist, "Suppressing photochemical reactions with quantized light fields," Nat. Commun. **7**, 13841 (2016).

[21] J. Galego, F. J. Garcia-Vidal, and J. Feist, "Many-molecule reaction triggered by a single photon in polaritonic chemistry," Phys. Rev. Lett. **119**, 136001 (2017).

[22] J. Galego, C. Climent, F. J. Garcia-Vidal, and J. Feist, "Cavity Casimir-Polder forces and their effects in ground-state chemical reactivity," Phys. Rev. X **9**, 021057 (2019).

[23] C. Schäfer, M. Ruggenthaler, V. Rokaj, and A. Rubio, "Relevance of the quadratic diamagnetic and self-polarization terms in cavity quantum electrodynamics," ACS Photonics **7**, 975–990 (2020).

[24] C. Schäfer, J. Flick, E. Ronca, P. Narang, and A. Rubio, "Shining light on the microscopic resonant mechanism responsible for cavity-mediated chemical reactivity," Nat. Commun. **13**, 7817 (2022).

[25] J. A. Campos-Gonzalez-Angulo, R. F. Ribeiro, and J. Yuen-Zhou, "Resonant catalysis of thermally activated chemical reactions with vibrational polaritons," Nat. Commun. **10**, 4685 (2019).

[26] T. E. Li, A. Nitzan, and J. E. Subotnik, "Collective vibrational strong coupling effects on molecular vibrational relaxation and energy transfer: Numerical insights via cavity molecular dynamics simulations," Angew. Chem., Int. Ed. **133**, 15661–15668 (2021).

[27] T. E. Li, A. Nitzan, and J. E. Subotnik, "On the origin of ground-state vacuum-field catalysis: Equilibrium consideration," J. Chem. Phys. **152**, 234107 (2020).

[28] J. A. Campos-Gonzalez-Angulo and J. Yuen-Zhou, "Polaritonic normal modes in transition state theory," J. Chem. Phys. **152**, 161101 (2020).

[29] X. Li, A. Mandal, and P. Huo, "Theory of mode-selective chemistry through polaritonic vibrational strong coupling," J. Phys. Chem. Lett. **12**, 6974–6982 (2021).

[30] X. Li, A. Mandal, and P. Huo, "Cavity frequency-dependent theory for vibrational polariton chemistry," Nat. Commun. **12**, 1315 (2021).

[31] P.-Y. Yang and J. Cao, "Quantum effects in chemical reactions under polaritonic vibrational strong coupling," J. Phys. Chem. Lett. **12**, 9531–9538 (2021).

[32] J. Sun and O. Vendrell, "Suppression and enhancement of thermal chemical rates in a cavity," J. Phys. Chem. Lett. **13**, 4441–4446 (2022).

[33] L. P. Lindoy, A. Mandal, and D. R. Reichman, "Resonant cavity modification of ground-state chemical kinetics," J. Phys. Chem. Lett. **13**, 6580–6586 (2022).

[34] M. R. Fiechter, J. E. Runeson, J. E. Lawrence, and J. O. Richardson, "How quantum is the resonance behavior in vibrational polariton chemistry?" J. Phys. Chem. Lett. **14**, 8261–8267 (2023).

[35] M. Du, Y. R. Poh, and J. Yuen-Zhou, "Vibropolaritonic reaction rates in the collective strong coupling regime: Pollak–Grabert–Hänggi theory," J. Phys. Chem. C **127**, 5230–5237 (2023).

[36] J. Sun and O. Vendrell, "Modification of thermal chemical rates in a cavity via resonant effects in the collective regime," J. Phys. Chemi. Lett. **14**, 8397–8404 (2023).

[37] D. S. Wang, T. Neuman, S. F. Yelin, and J. Flick, "Cavity-modified unimolecular dissociation reactions via intramolecular vibrational energy redistribution," J. Phys. Chem. Lett. **13**, 3317–3324 (2022).

[38] J. Fregoni, F. J. Garcia-Vidal, and J. Feist, "Theoretical challenges in polaritonic chemistry," ACS Photonics **9**, 1096–1107 (2022).

[39] E. W. Fischer, J. Anders, and P. Saalfrank, "Cavity-altered thermal isomerization rates and dynamical resonant localization in vibro-polaritonic chemistry," J. Chem. Phys. **156**, 154305 (2022).

[40] E. W. Fischer and P. Saalfrank, "Cavity-catalyzed hydrogen transfer dynamics in an entangled molecular ensemble under vibrational strong coupling," Phys. Chem. Chem. Phys. **25**, 11771–11779 (2023).

[41] I. Sokolovskii and G. Groenhof, "Non-hermitian molecular dynamics simulations of exciton-polaritons in lossy cavities," arXiv preprint arXiv:2311.13453 (2023).

[42] F. Pavošević, R. L. Smith, and A. Rubio, "Computational study on the catalytic control of endo/exo Diels-Alder reactions by cavity quantum vacuum fluctuations," Nat. Commun. **14**, 2766 (2023).

[43] D. Hu, W. Ying, and P. Huo, "Resonance enhancement of vibrational polariton chemistry obtained from the mixed quantum-classical dynamics simulations," J. Phys. Chem. Lett. **14**, 11208–11216 (2023).

[44] A. Mandal, S. Montillo Vega, and P. Huo, "Polarized fock states and the dynamical Casimir effect in molecular cavity quantum electrodynamics," J. Phys. Chem. Lett. **11**, 9215–9223 (2020).

[45] A. Mandal, X. Li, and P. Huo, "Theory of vibrational polariton chemistry in the collective coupling regime," J. Chem. Phys. **156** (2022).

[46] A. Mandal, M. A. Taylor, B. M. Weight, E. R. Koessler, X. Li, and P. Huo, "Theoretical advances in polariton chemistry and molecular cavity quantum electrodynamics," Chem. Rev. **123**, 9786–9879 (2023).

[47] J. Campos-Gonzalez-Angulo, Y. Poh, M. Du, and J. Yuen-Zhou, "Swinging between shine and shadow: Theoretical advances on thermally activated vibropolaritonic chemistry." J. Chem. Phys. **158**, 230901–230901 (2023).

[48] M. Ruggenthaler, D. Sidler, and A. Rubio, "Understanding polaritonic chemistry from ab initio quantum electrodynamics," Chem. Rev. **123**, 11191–11229 (2023).

[49] L. P. Lindoy, A. Mandal, and D. R. Reichman, "Quantum dynamical effects of vibrational strong coupling in chemical reactivity," Nat. Commun. **14**, 2733 (2023).

[50] W. Ying and P. Huo, "Resonance theory and quantum dynamics simulations of vibrational polariton chemistry," J. Chem. Phys. **159**, 084104 (2023).

[51] Y. Ke and J. Richardson, "Insights into the mechanisms of optical cavity-modified ground-state chemical reactions," (2023).

[52] L. P. Lindoy, A. Mandal, and D. R. Reichman, "Investigating the collective nature of cavity-modified chemical kinetics under vibrational strong

https://doi.org/10.26434/chemrxiv-2024-nfmpk **ORCID:** https://orcid.org/0000-0001-6625-3981 Content not peer-reviewed by ChemRxiv. **License:** CC BY 4.0

coupling," Nanophotonics (2024).
[53]Y. Tanimura, "Numerically "exact" approach to open quantum dynamics: The hierarchical equations of motion (HEOM)," J. Chem. Phys. **153**, 020901 (2020).
[54]J. Flick, M. Ruggenthaler, H. Appel, and A. Rubio, "Atoms and molecules in cavities, from weak to strong coupling in quantum-electrodynamics (QED) chemistry," Proc. Natl. Acad. Sci. USA **114**, 3026–3034 (2017).
[55]V. Rokaj, D. M. Welakuh, M. Ruggenthaler, and A. Rubio, "Light–matter interaction in the long-wavelength limit: no ground-state without dipole self-energy," J. Phys. B: At. Mol. Opt. Phys. **51**, 034005 (2018).
[56]A. Erpenbeck, C. Schinabeck, U. Peskin, and M. Thoss, "Current-induced bond rupture in single-molecule junctions," Phys. Rev. B **97**, 235452 (2018).
[57]J. Hu, R.-X. Xu, and Y. Yan, "Communication: Padé spectrum decomposition of Fermi function and Bose function," J. Chem. Phys. **133**, 101106 (2010).
[58]M. Xu, Y. Yan, Q. Shi, J. Ankerhold, and J. Stockburger, "Taming quantum noise for efficient low temperature simulations of open quantum systems," Phys. Rev. Lett. **129**, 230601 (2022).
[59]R. Borrelli, "Density matrix dynamics in twin-formulation: An efficient methodology based on tensor-train representation of reduced equations of motion," J. Chem. Phys. **150**, 234102 (2019).
[60]R. Borrelli and M. F. Gelin, "Finite temperature quantum dynamics of complex systems: Integrating thermo-field theories and tensor-train methods," WIREs Comput Mol Sci , e1539 (2021).
[61]Y. Ke, R. Borrelli, and M. Thoss, "Hierarchical equations of motion approach to hybrid fermionic and bosonic environments: Matrix product state formulation in twin space," J. Chem. Phys. **156**, 194102 (2022).
[62]U. Schollwöck, "The density-matrix renormalization group in the age of matrix product states," Ann. Phys. (NY) **326**, 96–192 (2011).
[63]I. V. Oseledets, "Tensor-train decomposition," SIAM J. Sci. Comput. **33**, 2295–2317 (2011).
[64]J. Haegeman, C. Lubich, I. Oseledets, B. Vandereycken, and F. Verstraete, "Unifying time evolution and optimization with matrix product states," Phys. Rev. B **94**, 165116 (2016).
[65]S. Paeckel, T. Köhler, A. Swoboda, S. R. Manmana, U. Schollwöck, and C. Hubig, "Time-evolution methods for matrix-product states," Ann. Phys. (NY) **411**, 167998 (2019).
[66]A. J. Dunnett and A. W. Chin, "Efficient bond-adaptive approach for finite-temperature open quantum dynamics using the one-site time-dependent variational principle for matrix product states," Phys. Rev. B **104**, 214302 (2021).
[67]G. Stock and M. Thoss, "Classical description of nonadiabatic quantum dynamics," Adv. Chem. Phys. **131**, 243–375 (2005).
[68]R. Grunwald, A. Kelly, and R. Kapral, "Quantum dynamics in almost classical environments," in Energy Transfer Dynamics in Biomaterial Systems (Springer, 2009) pp. 383–413.
[69]J. Echave and D. C. Clary, "Potential optimized discrete variable representation," Chem. Phys. Lett. **190**, 225–230 (1992).
[70]W. H. Miller, S. D. Schwartz, and J. W. Tromp, "Quantum mechanical rate constants for bimolecular reactions," J. Chem. Phys. **79**, 4889–4898 (1983).
[71]I. R. Craig, M. Thoss, and H. Wang, "Proton transfer reactions in model condensed-phase environments: Accurate quantum dynamics using the multilayer multiconfiguration time-dependent Hartree approach," J. Chem. Phys. **127**, 144503 (2007).
[72]L. Chen and Q. Shi, "Quantum rate dynamics for proton transfer reactions in condensed phase: The exact hierarchical equations of motion approach," J. Chem. Phys. **130**, 134505 (2009).
[73]Y. Ke, C. Kaspar, A. Erpenbeck, U. Peskin, and M. Thoss, "Nonequilibrium reaction rate theory: Formulation and implementation within the hierarchical equations of motion approach," J. Chem. Phys. **157**, 034103 (2022).
[74]B. Xiang, J. Wang, Z. Yang, and W. Xiong, "Nonlinear infrared polaritonic interaction between cavities mediated by molecular vibrations at ultrafast time scale," Sci. Adv. **7**, eabf6397 (2021).
[75]D. Xu, A. Mandal, J. M. Baxter, S.-W. Cheng, I. Lee, H. Su, S. Liu, D. R. Reichman, and M. Delor, "Ultrafast imaging of polariton propagation and interactions," Nat. Commun. **14**, 3881 (2023).
[76]P. V. Parandekar and J. C. Tully, "Detailed balance in Ehrenfest mixed quantum-classical dynamics," J. Chem. Theory Comput. **2**, 229–235 (2006).
[77]J. E. Runeson, J. E. Lawrence, J. R. Mannouch, and J. O. Richardson, "Explaining the Efficiency of Photosynthesis: Quantum Uncertainty or Classical Vibrations?" J. Phys. Chem. Lett. **13**, 3392–3399 (2022).
[78]G. Amati, J. R. Mannouch, and J. O. Richardson, "Detailed balance in mixed quantum–classical mapping approaches," J. Chem. Phys. **159**, 214114 (2023), 2309.04686.
[79]J. E. Runeson and J. O. Richardson, "Spin-mapping approach for nonadiabatic molecular dynamics," J. Chem. Phys. **151**, 044119 (2019), arXiv:1904.08293 [physics.chem-ph].
[80]J. E. Runeson and J. O. Richardson, "Generalized spin mapping for quantum-classical dynamics," J. Chem. Phys. **152**, 084110 (2020), arXiv:1912.10906 [physics.chem-ph].
[81]J. R. Mannouch and J. O. Richardson, "A mapping approach to surface hopping," J. Chem. Phys. **158**, 104111 (2023), arXiv:2212.11773 [physics.chem-ph].

https://doi.org/10.26434/chemrxiv-2024-nfmpk **ORCID:** https://orcid.org/0000-0001-6625-3981 Content not peer-reviewed by ChemRxiv. **License:** CC BY 4.0